Rotationally Resolved State-to-State Photoelectron Study of Molybdenum Monoxide Cation (MoO(+))

ARTICLE *in* THE JOURNAL OF PHYSICAL CHEMISTRY A · SEPTEMBER 2015

Impact Factor: 2.69 · DOI: 10.1021/acs.jpca.5b07939

5 AUTHORS, INCLUDING:

C. Y. Ng

University of California, Davis

390 PUBLICATIONS **7,065** CITATIONS

SEE PROFILE

THE JOURNAL OF PHYSICAL CHEMISTRY A

Article

pubs.acs.org/JPCA

Rotationally Resolved State-to-State Photoelectron Study of Molybdenum Monoxide Cation (MoO^+)

Zhihong Luo,[†,‡] Yih-Chung Chang,[†] Yi Pan,[§] Kai-Chung Lau,[*,§] and C. Y. Ng[*,†]

[†]Department of Chemistry, University of California, Davis, California 95616, United States

[‡]Department of Physics, Tsinghua University, Beijing 100084, China

[§]Department of Biology and Chemistry, City University of Hong Kong, 80 Tat Chee Avenue, Kowloon, Hong Kong

ABSTRACT: By employing the two-color visible−ultraviolet (vis−UV) laser pulsed field ionization−photoelectron (PFI−PE) measurement, we have obtained rotationally selected and resolved photoelectron spectra for the $MoO^+(X^4\Sigma^-;\ v^+ = 0, 1,$ and $2)$ and $MoO^+(a^2\Delta_{3/2,5/2};\ v^+ = 0$ and $1)$ cationic states. The unambiguous rotational assignments have made possible the determination of highly precise values for the band origin $\nu_{00}^+ = 60\,147.9 \pm 0.8$ cm^{-1}, rotation constant $B_0^+ = 0.4546 \pm 0.0006$ cm^{-1}, spin−spin coupling constant $\lambda = 26.454 \pm 0.017$ cm^{-1}, and bond length $r_e^+ = 1.642 \pm 0.001$ Å for the $MoO^+(X^4\Sigma^-)$ ground state; $\nu_{00}^+ = 60\,556.4 \pm 0.8$ cm^{-1}, $B_0^+ = 0.4711 \pm 0.0005$ cm^{-1}, and $r_0^+ = 1.613 \pm 0.001$ Å for the MoO^+ $(a^2\Delta_{3/2})$ excited state; and $\nu_{00}^+ = 61\,718.2 \pm 0.8$ cm^{-1}, $B_0^+ = 0.4695 \pm 0.0006$ cm^{-1}, and $r_0^+ = 1.616 \pm 0.001$ Å for the MoO^+ $(a^2\Delta_{5/2})$ excited state. The ionization energy (IE) for MoO is determined to be IE(MoO) = 60 095.1 ± 0.8 cm^{-1} [7.4508 ± 0.0001 eV]. Furthermore, the vibrational constants are determined as $\omega_e^+ = 1000 \pm 9$ cm^{-1} and $\omega_e^+x_e^+ = 5 \pm 3$ cm^{-1} for $MoO^+(X^4\Sigma^-)$; the vibration spacing $\Delta G(1/2)$ for $MoO^+(a^2\Delta_{3/2})$ is also measured as 1065 ± 4 cm^{-1}. On the basis of the thermochemical cycle, together with the known IE(Mo) and the IE(MoO) determined in this study, the difference of 0 K bond dissociation energy for MoO^+ and that for MoO is determined to be $D_0(Mo^+-O) - D_0(Mo-O) = IE(Mo) - IE(MoO) = -2890.8 \pm 0.9$ cm^{-1} [−0.3584 ± 0.0001 eV]. The energetic and spectroscopic values determined here have been used for benchmarking calculations at the CCSDTQ/CBS level of theory. The CCSDTQ/CBS predictions, IE(MoO) = 7.457 eV, $r_e^+ = 1.651$ Å, $\omega_e^+ = 974$ cm^{-1}, $D_0(Mo-O) = 5.386$, and $D_0(Mo^+-O) = 5.015$ eV, are found to be in good agreement with the vis−UV PFI−PE measurements. We also recommend a set of equally reliable CCSDTQ/CBS thermochemical values for MoO and MoO^+: $\Delta H^\circ_{f0}(MoO) = 383.7$, $\Delta H^\circ_{f298}(MoO) = 384.0$, $\Delta H^\circ_{f0}(MoO^+) = 1103.2$, and $\Delta H^\circ_{f298}(MoO^+) = 1103.5$ kJ mol^{-1}.

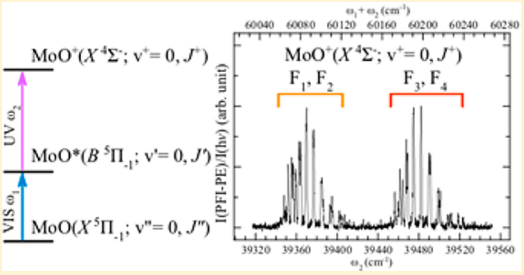

1. INTRODUCTION

Transition-metal-containing molecules play an important role in catalysis, astrophysics, and organometallic chemistry. The availability of partially filled d-orbitals makes them good electron donors as well as acceptors, facilitating the catalytic function in chemical synthesis. The unpaired d-electrons in transition-metal elements are also known to give rise to low-lying spin multiplicity states for transition-metal-containing compounds, particularly in the case of forming chemical bonds with a molybdenum atom, Mo ($5s^14d^5$), where both the 5s and 4d subshells are half-filled in its ground state. Accurate energetic and spectroscopic predictions of low-lying multiplicity states require the inclusion of extensive configuration interactions. This presents difficulties for accurate theoretical calculations of chemical properties for transition-metal-containing species. The careful benchmarking of theoretical predictions by highly reliable experimental measurements is a prerequisite for the establishment of accurate ab initio quantum calculation procedures.

To obtain accurate energetic and spectroscopic data, such as ionization energies (IEs), 0 K bond dissociation energies (D_0's), rotational and vibrational constants, and fine-structure splitting constants, for transition-metal-containing species and their cations, we have undertaken rotationally resolved state-to-state photoionization and photoelectron studies of a series of 3d-transition-metal carbides, nitrides, and oxides, including FeC, NiC, CoC, TiC, TiO, VC, and VN.[1−7] Parallel to this experimental effort, we have also been performing high-level ab initio quantum calculations based on the coupled cluster theory with electronic excitations up to quadruple (CCSDTQ), along with applying the complete basis set (CBS) technique (CCSDT/CBS). Highly precise energetic data and spectroscopic constants for FeC^+, NiC^+, CoC^+, and VC^+ cations obtained in two-color visible−ultraviolet (vis−UV) pulsed field ionization−photoelectron (PFI−PE) measurements were compared to theoretical CCSDTQ/CBS predictions, showing that the CCSDTQ/CBS procedure is capable of providing reliable energetic and spectroscopic predictions for these 3d-transition-metal-containing molecules and their cations.[6,8−10]

Special Issue: Piergiorgio Casavecchia and Antonio Lagana Festschrift

Received: August 14, 2015
Revised: September 23, 2015

DOI: 10.1021/acs.jpca.5b07939
J. Phys. Chem. A XXXX, XXX, XXX−XXX

The error limits for CCSDTQ/CBS IE predictions are found to fall within ±30 meV. We have recently extended the vis−UV PFI−PE measurements to include 4d-transition-metal-containing carbides and oxides, such as NbC and ZrO, aiming to further test the accuracy of the CCSDTQ/CBS procedure.[11,12]

The primary motivation of the present report is to present the energetic and spectroscopic data for the MoO/MoO^+ system obtained in rotationally selected and resolved vis−UV PFI−PE measurements of MoO. Previous spectroscopic measurements on the MoO/MoO^+ system have been focused on the neutral MoO molecule. The spectroscopic data for MoO^+ cation remain mostly unknown. Harmrick et al. have performed a jet-cooled spectroscopic study of MoO and identified the $A'^5\Delta-X^5\Pi$, $B'^5\Pi-X^5\Pi$, and $B^5\Pi-X^5\Pi$ excitation bands for MoO in the visible region.[13] Kuzyakov et al. have also examined the visible electronic spectra of MoO by employing the intracavity absorption technique.[14] Most recently, Harms et al. reported a combined theoretical and experimental study on the $c-a$ excitation band in the infrared region.[15] The photoelectron detachment study of MoO^- anion has confirmed that the neutral MoO(X) ground state is of $^5\Pi$ symmetry.[16] The two-color vis−UV photoionization study of MoO performed by Loock et al. provided a highly precise IE(MoO) value of 7.4504 ± 0.0005 eV [60 092 ± 4 cm^{-1}].[17] On the theoretical front, several theoretical investigations have been made previously on the low-lying multiplicity states of neutral MoO.[18−22]

In the present rotationally resolved PFI−PE study, we have determined the term symmetry of the ground-state $MoO^+(X)$ cation to be $^4\Sigma^-$ and identified the spin−orbit components of a low-lying $MoO^+(a^2\Delta)$ ion state. The rotational and vibrational constants for $MoO^+(X^4\Sigma^-)$ and $MoO^+(a^2\Delta)$ are determined in this study. The IE(MoO) value obtained here is in excellent agreement with the photoionization study of Loock et al.,[17] but has a smaller error limit. In this study, we have also performed CCSDTQ/CBS calculations on the MoO/MoO^+ system for comparison with the experimental PFI−PE measurements. In addition to the IE and D_0 predictions, we have obtained reliable CCSDTQ/CBS values for the 0 and 298 K heats of formation (ΔH°_{fT}, T = 0 and 298 K) for MoO and MoO^+. The highly precise energetic and spectroscopic data for the MoO/MoO^+ system presented here are expected to contribute to the experimental database needed for validating density functional and semiempirical computation procedures for providing energetic and structural predictions of larger 3d- and 4d-transition-metal-containing compounds and their cations.

2. EXPERIMENTAL AND THEORETICAL CONSIDERATIONS

2.1. Experiment Methods. The experiment arrangement and procedures employed are similar to those reported in detail previously;[1,3,11] thus, only a brief description is given below. The photoion−photoelectron apparatus used in this experiment consists of a supersonically cooled laser ablation beam source for the preparation of cold MoO molecules, a time-of-flight (TOF) ion mass spectrometer for photoion detection, and a TOF photoelectron spectrometer for PFI−PE detection. Two independently tunable dye lasers [Lambda physics model FL2002; optical bandwidth, 0.4 cm^{-1} full-width at half-maximum (fwhm); and Lambda physics model FL3002, optical bandwidth, 0.2 cm^{-1} (fwhm)] pumped by the same Nd:YAG laser (Spectra Physics Model: PRO-290; repetition rate, 30 Hz) were employed to generate the respective vis ω_1 and UV ω_2 outputs as required by the experiment.

The MoO molecules were prepared by reactions between gaseous Mo atoms and O_2. The gaseous Mo atoms were produced by laser ablation of a translating and rotating Mo rod (99.9% purity); O_2 molecules were introduced as an O_2/He (<1% O_2 in He) gaseous mixture into the reaction channel of the laser ablation beam source by a pulsed valve (repetition rate, 30 Hz; nozzle diameter, 1 mm; total stagnation pressure, 40 psi). The frequency-doubled 532 nm output (pulse energy, 2 mJ) of a Nd:YAG laser was used for ablation of the Mo rod. The MoO molecules formed in the reaction channel were further cooled by supersonic expansion and skimmed by a conical skimmer (diameter, 2 mm) before entering into the photoionization/photoexcitation (PI/PEX) center, where the MoO sample in the form of a pulsed molecular beam intersects the vis ω_1 and UV ω_2 laser beams at 90°. The cold MoO molecules were first excited to a selected intermediate MoO* state by vis ω_1 followed by UV ω_2 excitation for vis−UV photoionization or vis−UV PFI−PE measurements.

In photoionization measurements, a dc electric field was applied to the PI/PEX region, to extract and guide the photoions toward the TOF mass spectrometer for detection by the ion microchannel plate (MCP) detector. A pulsing scheme was used in the PFI−PE measurement. The PI/PEX region was kept field free during the vis−UV photoexcitation in order to minimize the destruction of high-n Rydberg molecules. A 0.1 V/cm electric pulse was applied to the PI/PEX region at a delay of 200 ns with respect to the UV ω_2 pulse to disperse the prompt background electrons. The PFI electric pulse of 0.7 V/cm was applied to the PI/PEX region to Stark ionize the high-n Rydberg molecules at a delay of 2.2 μs with respect to the UV ω_2 pulse. The PFI−PEs thus produced were also extracted by the 0.7 V/cm PFI field into the TOF photoelectron spectrometer for detection by the electron MCP detector. All spectra presented in this study represent the average of at least three reproducible scans. All IE values for the formation of MoO^+ ionic states reported here have been corrected for the Stark shift induced by the pulsed electric fields employed for PFI−PE detection.[3]

2.2. Theoretical Considerations. In the coupled cluster calculations using the CCSDTQ/CBS procedure, we have chosen to use the partially unrestricted implementation, conventionally labeled as ROHF-UCCSD(T). This method is based on restricted open-shell Hartree−Fock (ROHF) orbitals and relaxes the spin restriction throughout the calculations.[23,24]

The CCSDTQ/CBS calculations involve approximation to the CBS limit at the CCSD(T) level of theory. As there is no all-electron basis set available for Mo, the pseudopotential (PP) basis sets[25] are employed in the CCSDTQ/CBS predictions. The ground-state structures of the MoO($X^5\Pi$) and $MoO^+(X^4\Sigma^-)$ have been optimized at the CCSD(T) level, proceeding from aug-cc-pwCVTZ(-PP), to aug-cc-pwCVQZ(-PP), and to aug-cc-pwCV5Z(-PP)[25,26] basis sets. The geometry optimizations correlate the 1s2s2p electrons on oxygen and 4s4p4d5s electrons on molybdenum. The [Ar]$3d^{10}$ core electrons on molybdenum are simulated by the scalar-relativistic pseudopotentials.[26] The total CCSD(T) energies are used to extrapolate the energies at the CBS limit ($E_{\text{extrapolated CBS}}$) by the two schemes:

(i) A three-point extrapolation scheme[27] using the mixed exponential−Gaussian function of the form

DOI: 10.1021/acs.jpca.5b07939
J. Phys. Chem. A XXXX, XXX, XXX−XXX

$$E(X) = E_{\text{extrapolatedCBS}} + B\exp[-(X-1)] + C\exp[-(X-1)^2] \quad (1)$$

where X = 3, 4, and 5 represent the use of the aug-cc-pwCVTZ(-PP), aug-cc-pwCVQZ(-PP), and aug-cc-pwCV5Z(-PP) basis sets, respectively.

(ii) A two-point extrapolation scheme[28,29] using the simple power function involving the reciprocal of X

$$E(X) = E_{\text{extrapolated CBS}} + \frac{B}{X^3} \quad (2)$$

Here X = 4 or 5 represents the use of aug-cc-pwCVQZ(-PP) or aug-cc-pwCV5Z(-PP) basis sets, respectively. Previous calculations on FeC/FeC$^+$,[8] NiC/NiC$^+$,[9] CoC/CoC$^+$,[10] VC/VC$^+$,[6] and other main group molecules[30−34] reveal that the difference of extrapolated energetics between the two-point and three-point extrapolation schemes are typically small; thus, the average of the two extrapolated energies are adopted.

The higher-order energy correction (HOC) incorporates higher-order triple and quadruple excitations, where the full triple excitation effect is estimated by the difference between CCSDT and CCSD(T) energies and the iterative quadruple excitations are estimated as the difference of CCSDTQ and CCSDT energies. The HOC for MoO/MoO$^+$ is taken as

$$E_{\text{HOC}} = E_{\text{CCSDT/aug-cc-pVQZ(-PP)}} - E_{\text{CCSD(T)/aug-cc-pVQZ(-PP)}} + E_{\text{CCSDTQ/cc-pVTZ(-PP)}} - E_{\text{CCSDT/cc-pVTZ(-PP)}} \quad (3)$$

The electronic correlation contributions between core and valence electrons and those within core electrons have already been included in the single-point energy and geometrical optimization calculations at the CCSD(T) level. Additional core−valence electronic correlations (E_{CV}) from full triple excitations are obtained as the difference between CCSD(T) and CCSDT energies with the cc-pwCVTZ(-PP) basis set.[25,26]

The molecular spin−orbit couplings (E_{SO}'s) of MoO and MoO$^+$ are computed by first-order perturbation theory using the aug-cc-pVTZ-DK basis set. Spin−orbit matrix elements are computed among the components of the MoO/MoO$^+$ states using internally contracted MRCI wave functions.[35] In the spin−orbit calculations, the ground electronic state ($^5\Pi$) of MoO and the $^4\Sigma^-$, $^2\Delta$, $^4\Pi$, and $^2\Sigma^+$ states of MoO$^+$ are included; these electronics states are correlated with the asymptotic products of Mo(^{7}S) + O(^{3}P) and Mo$^+$(^{6}S) + O(^{3}P), respectively. The 2p electrons on O and the 4d5s electrons on Mo are included in the active space. No spin−orbit correction is found on Mo(^{7}S) and Mo$^+$(^{6}S).[36,37] The spin−orbit correction (0.93 kJ mol^{-1}) for atomic oxygen is directly taken from the experimental excitation energies tabulated by Moore.[38]

In the present work, the CCSD(T) single-point energy and correlation contributions are performed using the MOLPRO 2010.1 program,[39] and the CCSDT and CCSDTQ calculations are done with the string-based many-body MRCC program[40] interfaced with MOLRPO. The CCSDT, CCSDTQ, and MRCI(+Q) based ω_e and ω_e^+ values are obtained numerically, and the zero-point vibrational energy corrections (ΔE_{ZPVE}) are obtained from ω_e and ω_e^+ values at the CCSDTQ/cc-pVTZ(-PP) level. The ΔH°_{f0} and ΔH°_{f298} values for MoO and MoO$^+$ are obtained using the atomization scheme[41] and the following experimental thermochemical data[42] (in kJ mol^{-1}): ΔH°_{f0}(Mo) = 656.6, ΔH°_{f298}(Mo) = 658.1, ΔH°_{f0}(O) = 246.8, and ΔH°_{f298}(O) = 249.2. The 298 K thermal and enthalpy corrections to 0 K energies for elements and compounds are estimated using the methods adopted from Curtiss et al.[41]

3. RESULTS AND DISCUSSION

3.1. Neutral MoO*($B^5\Pi_{-1}$ − $X^5\Pi_{-1}$) Excitation Band.

Figure 1 depicts the P-branch rotational transitions of the neutral MoO*($B^5\Pi_{-1}$ − $X^5\Pi_{-1}$) excitation band obtained by scanning vis ω_1 in the range of 20 699−20 724 cm^{-1} and fixing UV ω_2 = 40 379.32 cm^{-1}. Hamrick et al. have previously performed a rotationally analysis of this $B^5\Pi_{-1}$ − $X^5\Pi_{-1}$ band and obtained highly precise rotation constants.[13] However, the band origin was not determined. The rotational energies of the $^5\Pi_{-1}$ states can be calculated by using the equation: $F(J) = BJ(J+1) \pm 1/2\, qBJ(J+1)$, where "+" and "−" are for the λ splitting a and b levels, respectively; B is the rotation constant, and q is the λ splitting constant. Thus, the transition energy is governed by eq 4

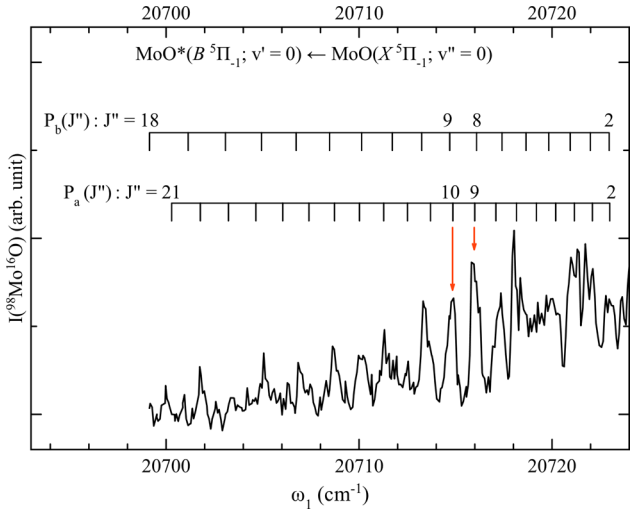

Figure 1. P-branch transitions of the MoO*($B^5\Pi_{-1}$) ← MoO($X^5\Pi_{-1}$) excitation band obtained by scanning the vis ω_1 in the range of 20 699−20 724 cm^{-1} and fixing UV ω_2 at 40 379.32 cm^{-1}.

$$\nu = \nu_{v'v''} + F(J') - F(J'') \quad (4)$$

where $F(J')$ and $F(J'')$ are the rotational energies for the final and initial states and $\nu_{v'v''} = \Delta T_{e'e''} + G(v') - G(v'')$ is the origin of the $v' \leftarrow v''$ vibrational band. Here, $\Delta T_{e'e''}$ is the transition energy between the electronic potential minimum of the final state and that of the initial state, and $G(v') = \omega_e'(v'+1/2) - \omega_e' x_e'(v'+1/2)^2$ and $G(v'') = \omega_e''(v''+1/2) - \omega_e'' x_e''(v''+1/2)^2$ are the corresponding vibrational energies of the final and initial states.

By using the rotational constants determined in the previous study[13] of Hamrick et al. (B' = 0.39293 ± 0.00017 cm^{-1}, q' = 0.01872 ± 0.00016 cm^{-1}, B'' = 0.41825 ± 0.00017 cm^{-1}, and q'' = 0.00062 ± 0.00014 cm^{-1}), we obtained ν_{00} = 20 724.7 ± 0.2 cm^{-1} and assigned the λ splitting $P_a(J'')$ and $P_b(J'')$ levels as marked on top of Figure 1. This assignment shows that rotational transitions observed in Figure 1 are not resolved and have considerable overlap between adjacent rotational transitions. Nevertheless, a careful analysis shows that the transition peaks at 20 714.82 and 20 715.98 cm^{-1} (marked by downward pointing red arrows in Figure 1) consist of only two rotational transitions, i.e., $P_a(10)$ and $P_b(9)$ for 20 714.82 cm^{-1} and $P_a(9)$ and $P_b(8)$ for 20715.98 cm^{-1}. Thus, by setting vis ω_1 at

DOI: 10.1021/acs.jpca.5b07939
J. Phys. Chem. A XXXX, XXX, XXX−XXX

20 714.82 and 20 715.98 cm^{-1} would allow the selection of MoO*($B^5\Pi_{-1}$; $v' = 0$, $J_a' = 9$, and $J_b' = 8$) and MoO*($B^5\Pi_{-1}$; $v' = 0$, $J_a' = 8$ and $J_b' = 7$), respectively, for photoionization or PFI–PE studies.

3.2. TOF Mass Spectrum. Figure 2a depicts the TOF mass spectrum recorded by fixing vis ω_1 = 20 714.82 cm^{-1} to excite

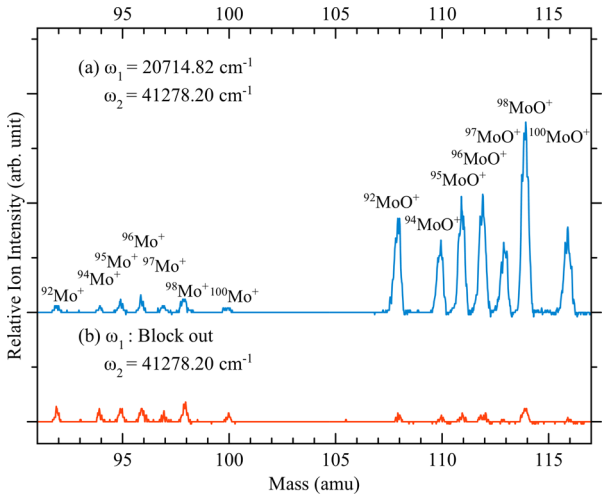

Figure 2. (a) TOF mass spectrum in the mass range of 91–117 amu, which was obtained by fixing vis ω_1 at 20 714.82 cm^{-1} and UV ω_2 at 41 278.20 cm^{-1}. (b) TOF spectrum obtained under the same experimental conditions except vis ω_1 was blocked.

MoO into the intermediate states MoO*($B^5\Pi_{-1}$; $v' = 0$, $J_a' = 9$ and $J_b' = 8$) via the $P_a(10)$ and $P_b(9)$ transitions, while fixing UV ω_2 = 41 278.20 cm^{-1} to photoionize excited MoO* molecules. In this experiment, the total energy, vis ω_1 + UV ω_2 = 61 993.02 cm^{-1}, is higher than the IE(Mo)[43] = 57 204.28 ± 0.32 cm^{-1} and IE(MoO)[17] = 60 092 ± 4 cm^{-1}. The seven Mo isotopes ^{92} Mo, ^{94} Mo, ^{95} Mo, ^{96} Mo, ^{97} Mo, ^{98} Mo, and ^{100} Mo and their natural abundances can be verified by scanning the Mo^+ atomic as well as the MoO^+ molecular ion intensities. The mass spectrum in Figure 2b was recorded under the same experimental conditions except vis ω_1 was blocked from entering the PI/PEX region. Without turning on the vis ω_1, the MoO^+ ion signal was found to reduce to near the noise level, whereas the Mo^+ atomic ion signals remain essentially unchanged. This observation indicates that the MoO^+ ion signals predominantly originated from the vis–UV two-color photoionization process, whereas the Mo^+ atomic ion signals were mostly generated by the UV two- and/or multiphoton ionization processes.

3.3. PFI–PE Spectra for $MoO^+(X^4\Sigma^-; v^+ = 0)$. As pointed out above, Loock et al. have reported an IE(MoO) value of 7.4504 ± 0.0005 eV [60 092 ± 4 cm^{-1}] based on two-color vis–UV photoionization efficiency measurements.[17] This work has been helpful for narrowing the energy range of the present vis–UV PFI–PE measurements. Figures 3 and 4 depict the PFI–PE spectra for $MoO^+(X^4\Sigma^-; v^+ = 0, J^+)$ (top black spectra) obtained by scanning UV ω_2 in the range of 39 317–39 551 cm^{-1}, while fixing vis ω_1 at 20 715.98 cm^{-1} and 20 714.82 cm^{-1}, respectively. By fixing vis ω_1 = 20 715.98 cm^{-1} (20 714.82 cm^{-1}), MoO is excited to the MoO*($B^5\Pi_{-1}$; $v' = 0$, $J_a' = 8$ and $J_b' = 7$) [MoO*($B^5\Pi_{-1}$; $v' = 0$, $J_a' = 9$ and $J_b' = 8$)] states via the $P_a(9)$ and $P_b(8)$ [$P_a(10)$ and $P_b(9)$] transitions.

The patterns of photoionization transitions of the PFI–PE spectra shown in Figures 3 and 4 are consistent with the $^4\Sigma^-$

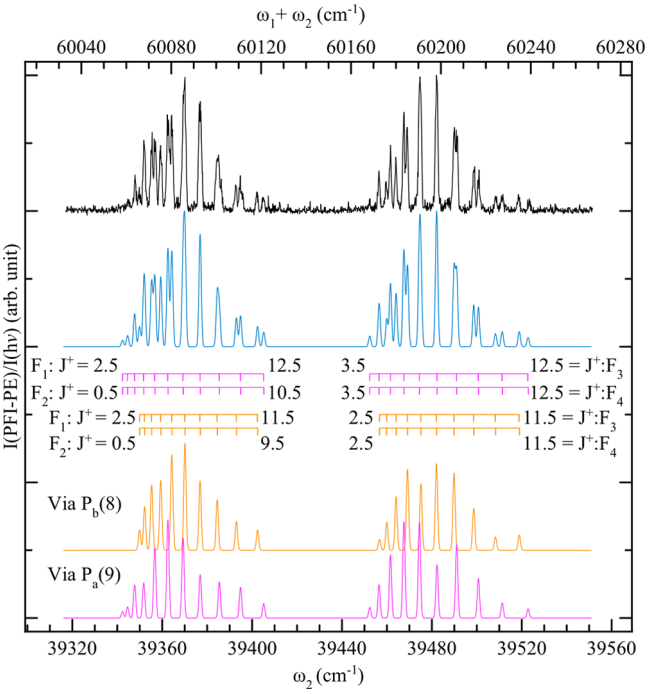

Figure 3. PFI–PE spectrum for $MoO^+(X^4\Sigma^-; v^+ = 0)$ obtained by fixing vis ω_1 at 20 715.98 cm^{-1} and scanning UV ω_2 in the range of 39 317–39 551 cm^{-1}. The vis ω_1 excited MoO to the intermediate state MoO*($B^5\Pi_{-1}$; $v' = 0$, $J_a' = 8$ and $J_b' = 7$) via $P_a(9)$ and $P_b(8)$ transitions, respectively. The blue curve is the sum of the best simulations of the $J_a' = 8 \rightarrow J^+$ and $J_b' = 7 \rightarrow J^+$ transitions, which are shown as the pink and orange curves, respectively. The simulations assume a Gaussian instrument profile of fwhm = 1.2 cm^{-1} for PFI–PE detection. The rotational assignments of the observed PFI–PE transitions are marked on top of the simulated curves for the $J_a' = 8 \rightarrow J^+$ and $J_b' = 7 \rightarrow J^+$ transitions.

term symmetry for the $MoO^+(X)$ ground state. As shown below, the $^4\Sigma^-$ state has the F_1, F_2, F_3, and F_4 transitions. The F_1 and F_2 ($^4\Sigma^-_{1/2}$) transitions as well as the F_3 and F_4 ($^4\Sigma^-_{3/2}$) transitions are very close in energy and thus appeared to overlap. Furthermore, the energy gap between the (F_1, F_2) and (F_3, F_4) transition components are about 100 cm^{-1}, which is expected to be significantly smaller than the spin–orbit splitting of low-lying electronic states of MoO^+. According to the convention of Herzberg, the total angular momentum J has four values in the $^4\Sigma^-$ state, $J = N + 3/2$ (F_1), $J = N + 1/2$ (F_2), $J = N - 1/2$ (F_3), and $J = N - 3/2$ (F_4). The effective Hamiltonian involved is given in eq 5.

$$H_{\text{eff}} = B\mathbf{N}^2 + (2/3)\lambda(3\mathbf{S}_z^2 - \mathbf{S}^2) + \gamma\mathbf{N}\cdot\mathbf{S} \quad (5)$$

where B is the rotational constant, λ the spin–spin coupling constant, and γ the spin-rotation coupling constant; $\mathbf{N}$ and $\mathbf{S}$ are the rotational and electron spin angular momenta, respectively.

By ignoring the spin-rotation coupling and using the pgopher software,[44] we have obtained the best simulated spectra (blue spectra) for the PFI–PE spectra of Figures 3 and 4, yielding ν_{00}^+ = 60 147.9 ± 0.8 cm^{-1}, B_0^+ = 0.4546 ± 0.0006 cm^{-1}, and λ = 26.454 ± 0.017 cm^{-1} for the formation of the $MoO^+(X^4\Sigma^-)$ ion ground state. From the rotation constant B_0^+, we have further obtained the bond length r_0^+ = 1.642 ± 0.001 Å for $MoO^+(X^4\Sigma^-)$. The total simulated spectrum (blue curve) of Figure 3 (Figure 4) represents the sum of the best simulated

DOI: 10.1021/acs.jpca.5b07939
J. Phys. Chem. A XXXX, XXX, XXX–XXX

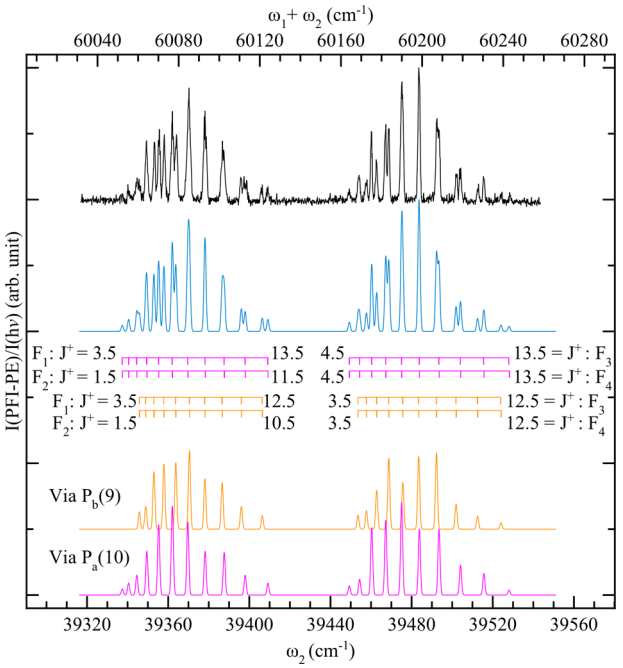

Figure 4. PFI–PE spectrum for $MoO^+(X^4\Sigma^-;\ v^+ = 0)$ obtained by fixing vis ω_1 at 20 714.82 cm^{-1} and scanning UV ω_2 in the range of 39 317–39 551 cm^{-1}. The vis ω_1 excited MoO to the intermediate state $MoO^*(B^5\Pi_{-1};\ v' = 0,\ J_a' = 9$ and $J_b' = 8)$ via $P_a(10)$ and $P_b(9)$ transitions, respectively. The blue curve is the sum of best simulations of the $J_a' = 9 \rightarrow J^+$ and $J_b' = 8 \rightarrow J^+$ transitions, which are shown as the pink and orange curves, respectively. The simulations assume a Gaussian instrument profile of fwhm = 1.2 cm^{-1} for PFI–PE detection. The rotational assignments of the observed PFI–PE transitions are marked on top of the simulated curves for the $J_a' = 9 \rightarrow J^+$ and $J_b' = 8 \rightarrow J^+$ transitions.

curves for photoionization transitions from the $J_a' = 8$ and $J_b' = 7$ ($J_a' = 9$ and $J_b' = 8$) levels to the J^+ levels of $MoO^+(X^4\Sigma^-;\ v^+ = 0)$, which are shown as the bottom pink and orange curves in Figure 3 (Figure 4), respectively. The simulation takes into account a Gaussian instrument profile of fwhm = 1.2 cm^{-1} for PFI–PE detection. While the J^+-rotational assignments as marked on top of the pink and orange simulated curves for the $J_a' = 8 \rightarrow J^+$ and $J_b' = 7 \rightarrow J^+$ photoionization transitions are based on the pgopher[44] fits to a standard transition formula, the intensities for the simulated J^+ rotational peaks are adjusted to give the best fits to the experimental PFI–PE intensities. Similar procedures for simulation of PFI–PE spectra and J^+-rotational assignments have been described in previous studies. Thus, the detailed procedures are not repeated here. The unambiguous J^+-rotational assignments achieved as marked on top the $J_a' = 8 \rightarrow J^+$ and $J_b' = 7 \rightarrow J^+$ [$J_a' = 9 \rightarrow J^+$ and $J_b' = 8 \rightarrow J^+$] simulated transitions in Figures 3 (Figures 4) have allowed us to determine the adiabatic IE of MoO [defined as the transition energy from $MoO(X^5\Pi_{-1};\ v'' = 0,\ J'' = 1)$ to the $J^+ = 0.5$ (F_1) level of $MoO^+(X^4\Sigma)$] to be 60095.1 ± 0.8 cm^{-1} [7.4508 ± 0.0001 eV]. This IE(MoO) value obtained here is in excellent agreement with that reported by Loock et al.,[17] but it has a smaller error limit.

For the detail of PFI–PE measurements, readers are referred to ref 45. The maximum transition intensities are observed at the J^+ = 6.5–8.5 and 7.5–9.5 states in Figures 3 and 4, respectively, with the J^+ intensity decreasing to lower as well as higher J^+ values. The intensity patterns of rotational transitions observed here are consistent those found previously in the PFI–PE study of other molecules,[1−5,7,11] indicating that the most favorable transitions are those with the smallest $|\Delta J^+|$ value. The maximum $|\Delta J^+| = |J^+ - J'|$ changes of 6.5–7.5 determined here for the MoO/MoO^+ photoionization system are also in line with those observed in previous studies.[11,46] For $\Delta J^+ < 0$ or $J^+ < J'$ transitions, the channel coupling mechanism[45,47,48] has been used to rationalize the observation of a wide range of ΔJ^+ rotational transitions. An inverse autoionization mechanism[48] has also been proposed for $\Delta J^+ > 0$ or $J^+ > J'$ transitions. Based on experimental observations,[1−5,7,11,12,46] the $\Delta J^+ > 0$ transition is less efficient than the $\Delta J^+ < 0$ transition. The $\Delta J^+ > 0$ transition is usually limited to $\Delta J^+ = 1$–3; but in an extreme case, such as TiC/TiC^+,[4] only the $\Delta J^+ < 0$ transition is observed and the $\Delta J^+ > 0$ transition is found to have negligible intensities.

The good agreement observed between the blue simulated curve and black PFI–PE curve can be taken as strong support of the rotational assignment and analysis. The Gaussian instrumentation width of 1.2 cm^{-1} (fwhm) used in the present simulation is close to the energy bandwidth for PFI–PE detection in previous vis–UV PFI–PE measurements of diatomic transition-metal oxides and carbides, indicating that the broadening or energy shift effect (see discussion below) on rotational transition energies due to Mo isotope substitution in the $MoO^+(X^4\Sigma^-;\ v^+ = 0)$ vibrational ground state is negligibly small compared to the instrumental bandwidth for PFI–PE detection. This observation is consistent with the isotope effect and the energy bandwidth of 1.2 cm^{-1} (fwhm) for PFI–PE detection observed in the previous PFI–PE measurement for $ZrO^+(X^2\Delta_{3/2,5/2};\ v^+ = 0$, 1, and 2).[12]

Based on the thermochemical cycle, together with the IE(MoO) = 7.4508 ± 0.0001 eV determined here and the known IE(Mo) = 7.09243 ± 0.00004 eV,[43] the difference of 0 K bond dissociation energy for MoO^+ and that for MoO is determined as $D_0(Mo^+-O) - D_0(Mo-O)$ = IE(Mo) − IE(MoO) = −0.3584 ± 0.0001 eV. This value is significantly smaller than the value of −0.70 ± 0.22 eV obtained based on the experimental values of $D_0(Mo^+-O)$ = 5.06 ± 0.02 eV and $D_0(Mo-O)$ = 5.76 ± 0.22 eV reported previously.[17,49,50]

3.4. PFI–PE Spectra for $MoO^+(X^4\Sigma^-;\ v^+ = 1$ and 2).

Figure 5a,b (Figure 5c,d) depict the PFI–PE spectra for $MoO^+(X^4\Sigma^-;\ v^+ = 1)$ [$MoO^+(X^4\Sigma^-;\ v^+ = 2)$] obtained by fixing vis ω_1 at 20 715.98 and 20 714.82 cm^{-1}, respectively, and scanning UV ω_2 in the range of 40 286–40 504 cm^{-1} [41 275–41 505 cm^{-1}]. The sharp peaks marked by asterisks in the spectra of Figure 5a–d are believed to be background peaks originating from two-photon and/or multiphoton ionization of Mo atoms. The rotational transition peaks of the PFI–PE spectra for the formation of $MoO^+(X^4\Sigma^-;\ v^+ = 1, 2)$ observed in these figures are similar to those for formation of $MoO^+(X^4\Sigma^-;\ v^+ = 0)$ of Figures 3 and 4, except that individual transition peaks in the spectra of Figures 5a–d are broader and exhibit multiple split peak structures. Similar observations have been reported previously in the PFI–PE study of the ZrO/ZrO^+ system,[12] where the broadening and split peak structures have been ascribed to the vibrational isotope shift effect due to the existence of Zr isotope substituted ZrO^+ ions.

The isotopic effects on the ion vibrational and rotational constants are given by eqs 6–8:

$$\omega_e^{+i} = (\mu^+/\mu^{+i})^{1/2}\omega_e^+ \quad (6)$$

DOI: 10.1021/acs.jpca.5b07939
J. Phys. Chem. A XXXX, XXX, XXX–XXX

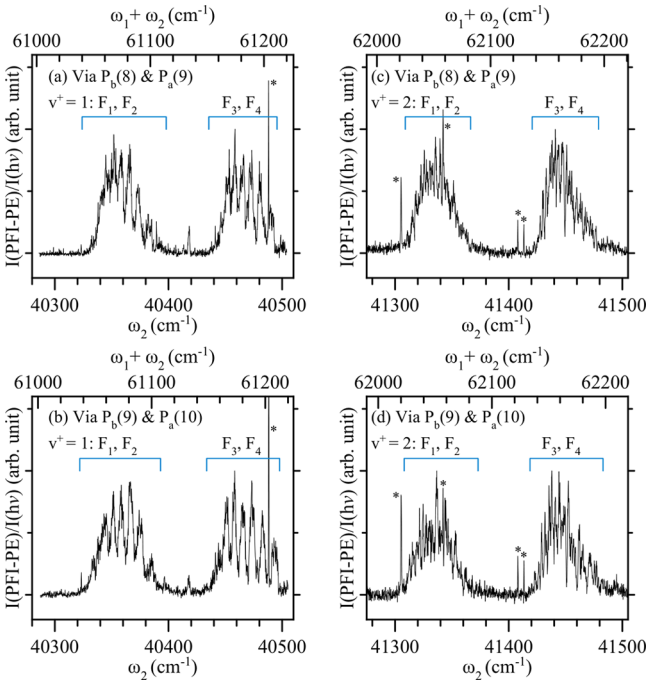

Figure 5. PFI–PE spectra for $MoO^+(X^4\Sigma^-; v^+ = 1)$ obtained by fixing vis ω_1 at (a) 20 715.98 and (b) 20 714.82 cm^{-1} and scanning UV ω_2 in the range of 40 286–40 504 cm^{-1}. The vis ω_1 = 20 715.98 cm^{-1} excited MoO to the intermediate states $MoO^*(B^5\Pi_{-1}; v' = 0, J_a' = 8$ and $J_b' = 7)$ via $P_a(9)$ and $P_b(8)$ transitions. The vis ω_1 = 20 714.82 cm^{-1} excited MoO to the intermediate state $MoO^*(B^5\Pi_{-1}; v' = 0, J_a' = 9$ and $J_b' = 8)$ states via $P_a(10)$ and $P_b(9)$ transitions. PFI–PE spectra for $MoO^+(X^4\Sigma^-; v^+ = 2)$ obtained by fixing vis ω_1 at (c) 20 715.98 and (d) 20 714.82 cm^{-1} and scanning UV ω_2 in the range of 41 275–41 505 cm^{-1}. The vis ω_1 = 20 715.98 cm^{-1} excited MoO to the intermediate state $MoO^*(B^5\Pi_{-1}; v' = 0, J_a' = 8$ and $J_b' = 7)$ via $P_a(9)$ and $P_b(8)$ transitions. The vis ω_1 = 20 714.82 cm^{-1} excited MoO to the intermediate states $MoO^*(B^5\Pi_{-1}; v' = 0, J_a' = 9$ and $J_b' = 8)$ via $P_a(10)$ and $P_b(9)$ transitions. The asterisks peaks are believed to originate from two-photon and/or photoionization of Mo atoms.

$$\omega_e^{+i}x_e^{+i} = (\mu^+/\mu^{+i})\omega_e^+x_e^+ \quad (7)$$

$$B_v^{+i} = (\mu^+/\mu^{+i})B_v^+ \quad (8)$$

where μ^+, ω_e^+, $\omega_e^+x_e^+$, and B_v^+ are the reduced mass, harmonic vibrational frequency, anharmonicity constant, and rotational constant, respectively, for $^{98}MoO^+$ of the major ^{98}Mo isotope; μ^{+i}, ω_e^{+i}, $\omega_e^{+i}x_e^{+i}$, and B_v^{+i} are those for MoO^+ of other Mo isotopes. These equations basically involve the scaling of the harmonic vibrational frequency, anharmonicity, and rotational constants by the reduced mass ratios (μ^+/μ^{+i}). That is, the existence of Mo isotope substituted MoO^+ can result in the change of vibrational frequency, anharmonicity constant, and rotational constant, giving rise to transition energy shifts (or PFI–PE transition energy broadening). Because ω_e^+ is significantly larger than $\omega_e^+x_e^+$ and B_v^+, the vibrational isotope shift induced by eq 6 is overwhelmingly more significant than those by eqs 7 and 8. Because the differences in natural abundances of the seven Mo isotopes are not large, the multiple split peaks structures revealed in the PFI–PE spectra shown in Figure 5a–d for the formation of vibrationally excited $MoO^+(X^4\Sigma^-; v^+ = 1$ and 2) states are more apparent compared to those observed in the previous PFI–PE measurement of vibrationally excited ZrO^+. As shown above, the transition line profiles observed in the origin PFI–PE bands of Figures 3 and 4, which involve the formation of the $MoO^+(X^4\Sigma^-; v^+ = 0)$ vibrational ground state, are found to have little isotope broadening effect. This observation is consistent with the fact that the rotational transition isotope shift effect (eq 8) is negligibly small compared to the energy bandwidth of PFI–PE detection achieved in the present study.

Based on the analysis of the PFI–PE spectra shown in Figures 3–5, the vibrational spacings are determined as $\Delta G(1/2) = 990 \pm 4$ cm^{-1} and $\Delta G(3/2) = 980 \pm 4$ cm^{-1} for $MoO^+(X^4\Sigma^-)$. By using the latter values and the standard equations

$$\Delta G(v^+ + 1/2) = G(v^+ + 1) - G(v^+) \quad (9)$$

$$G(v^+) = \omega_e^+(v^+ + 1/2) - \omega_e^+x_e^+(v^+ + 1/2)^2 \quad (10)$$

we have determined the harmonic vibrational frequency and anharmonicity constants to be $\omega_e^+ = 1000 \pm 9$ cm^{-1} and $\omega_e^+x_e^+ = 5 \pm 3$ cm^{-1} for $MoO^+(X^4\Sigma^-)$, respectively.

3.5. PFI–PE Spectra for $MoO^+(a^2\Delta_{3/2, 5/2}; v^+ = 0$ and 1). The PFI–PE spectrum for $MoO^+(a^2\Delta_{3/2}; v^+ = 0)$ shown as the top black curve in Figure 6 (Figure 7) was obtained by fixing vis

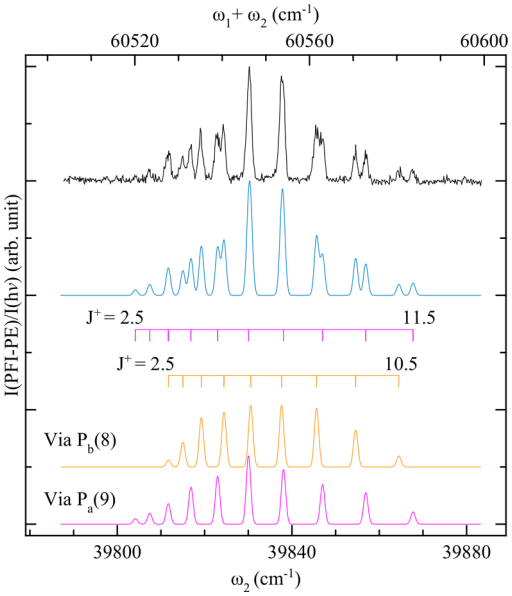

Figure 6. PFI–PE spectrum for $MoO^+(a^2\Delta_{3/2}; v^+ = 0)$ obtained by fixing vis ω_1 = 20 715.98 cm^{-1} and scanning UV ω_2 in the range of 39 788–39 883 cm^{-1}. The vis ω_1 excited MoO to the intermediate states $MoO^*(B^5\Pi_{-1}; v' = 0, J_a' = 8$ and $J_b' = 7)$ via the $P_a(9)$ and $P_b(8)$ transitions. The blue curve is the sum of the best simulations of the $J_a' = 8 \rightarrow J^+$ and $J_b' = 7 \rightarrow J^+$ transitions, which are shown as the pink and orange curves, respectively. The simulations assume a Gaussian instrument profile of fwhm = 1.2 cm^{-1} for PFI–PE detection.

ω_1 at 20 715.98 cm^{-1} (20 714.82 cm^{-1}) to excite the MoO molecule into intermediate state $MoO^*(B^5\Pi_{-1}; v' = 0, J_a' = 8$ and $J_b' = 7)$ [$MoO^*(B^5\Pi_{-1}; v' = 0, J_a' = 9$ and $J_b' = 8)$] via the respective $P_a(9)$ and $P_b(8)$ [$P_a(10)$ and $P_b(9)$] transitions. On the basis of least-squares fits of the observed transition energies to eq 4 and using $F(J^+) = B^+[J^+(J^+ + 1) - (\Omega^+)^2]$ for the rotational energy of the ionic state, we have obtained the band origin $\nu_{00}^+ = 60\,556.4 \pm 0.8$ cm^{-1} and rotation constant $B_0^+ = 0.4711 \pm 0.0005$ cm^{-1} for $MoO^+(a^2\Delta_{3/2}; v^+ = 0)$. The latter rotation constant yields a bond length of $r_0^+ = 1.613 \pm 0.001$ Å. The total simulated spectrum shown in blue in Figure 6 (Figure 7) is the sum of best simulated curves for the PFI–PE

DOI: 10.1021/acs.jpca.5b07939
J. Phys. Chem. A XXXX, XXX, XXX–XXX

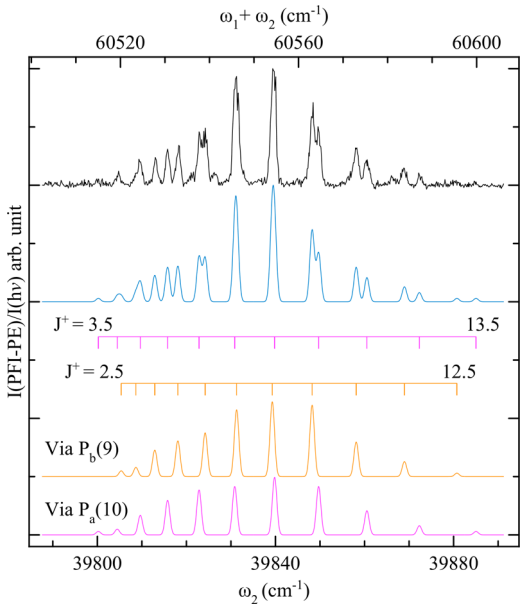

Figure 7. PFI–PE spectrum for $MoO^+(a^2\Delta_{3/2};\ v^+ = 0)$ obtained by fixing vis ω_1 = 20 714.82 cm^{-1} and scanning UV ω_2 in the range of 39 788–39 891 cm^{-1}. The vis ω_1 excited MoO to the intermediate states $MoO^*(B^5\Pi_{-1};\ v' = 0,\ J_a' = 9$ and $J_b' = 8)$ via $P_a(10)$ and $P_b(9)$ transitions. The blue curve is the sum of the best simulations of the $J_a' = 9 \rightarrow J^+$ and $J_b' = 8 \rightarrow J^+$ transitions, which are shown as the pink and orange curves, respectively. The simulations assume a Gaussian instrument profile of fwhm = 1.2 cm^{-1} for PFI–PE detection.

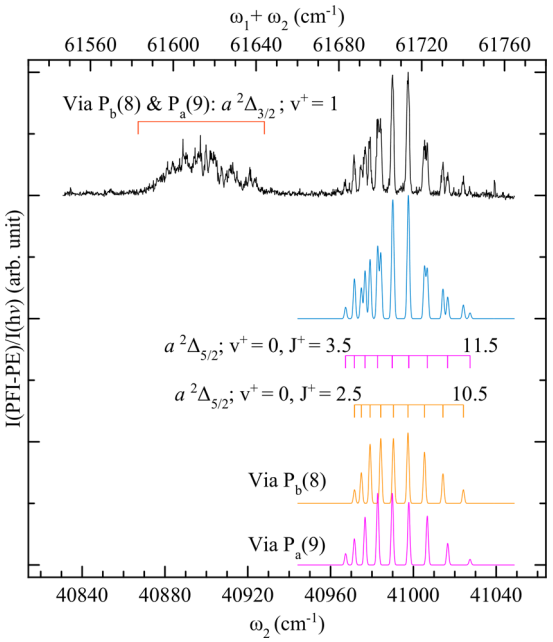

Figure 8. PFI–PE spectrum for $MoO^+(a^2\Delta_{3/2};\ v^+ = 1)$ and $MoO^+(a^2\Delta_{5/2};\ v^+ = 0)$ obtained by fixing vis ω_1 at 20 715.98 cm^{-1} and scanning UV ω_2 in the range of 40 831–41 049 cm^{-1}. The vis ω_1 excited MoO to the intermediate state $MoO^*(B^5\Pi_{-1};\ v' = 0,\ J_a' = 8$ and $J_b' = 7)$ via $P_a(9)$ and $P_b(8)$ transitions. The blue curve is the sum of the best simulations of the $J_a' = 8 \rightarrow J^+$ and $J_b' = 7 \rightarrow J^+$ transitions, which are shown as the pink and orange curves, respectively. The simulations assume a Gaussian instrument profile of fwhm = 1.2 cm^{-1} for PFI–PE detection.

transitions, $J_a' = 8 \rightarrow J^+$ and $J_b' = 7 \rightarrow J^+$ ($J_a' = 9 \rightarrow J^+$ and $J_b' = 8 \rightarrow J^+$), which are shown as the pink and orange curves, respectively.

Figure 8 (Figure 9) depicts the PFI–PE spectrum as the top black curve for the formation of $MoO^+(a^2\Delta_{3/2};\ v^+ = 1,\ J^+)$ and $MoO^+(a^2\Delta_{5/2};\ v^+ = 0,\ J^+)$ obtained by fixing vis ω_1 at 20 715.98 cm^{-1} (20 714.82 cm^{-1}) and scanning UV ω_2 in the range of 40 831–41 049 cm^{-1} (40 822–41 057 cm^{-1}). The PFI–PE spectra of Figures 8 and 9 display similar features. Similar to the PFI–PE spectrum for $MoO^+(X^4\Sigma^-;\ v^+ = 1$ and 2), the PFI–PE spectrum for $MoO^+(a^2\Delta_{3/2};\ v^+ = 1)$ exhibits multiple split peaks, which can be attributed to the vibrational isotope shift effect (eq 6). As expected, the PFI–PE spectra for $MoO^+(a^2\Delta_{3/2,5/2};\ v^+ = 0)$ were found to exhibit rotationally resolved transition peaks with little evidence of broadening due to the rotational isotope shift effect (eq 8). From the comparison of the PFI–PE spectra for $MoO^+(a^2\Delta_{3/2};\ v^+ = 0)$ shown in Figures 6 and 7 and those for $MoO^+(a^2\Delta_{3/2};\ v^+ = 1)$ depicted in Figures 8 and 9, the vibration spacing $\Delta G(1/2)$ is determined to be 1065 ± 4 cm^{-1} for $MoO^+(a^2\Delta_{3/2})$. This latter value is higher than the $\Delta G(1/2)$ value of 990 ± 4 cm^{-1} for $MoO^+(X^4\Sigma^-)$. The least-squares fitting of the rotationally resolved transition peaks yields the band origin $\nu_{00}^+ = 61718.2 \pm 0.8$ cm^{-1} and rotation constant $B_0^+ = 0.4695 \pm 0.0006$ cm^{-1} for $MoO^+(a^2\Delta_{5/2};\ v^+ = 0)$. This rotational constant gives a bond length of $r_0^+ = 1.616 \pm 0.001$ Å. The determination of the origins of the $MoO^+(a^2\Delta_{3/2,5/2};\ v^+ = 0)$ PFI–PE bands give the spin–orbit constant of $A = 580.9 \pm 0.8$ cm^{-1}. The total simulated blue spectrum, shown as the blue spectrum in Figure 8 (Figure 9), is the sum of best simulated curves for the PFI–PE transitions, $J_a' = 8 \rightarrow J^+$ and $J_b' = 7 \rightarrow J^+$ ($J_a' = 9 \rightarrow J^+$ and $J_b' = 8 \rightarrow J^+$) which are shown as the pink and orange curves, respectively. Because of the limited experimental sensitivity, the

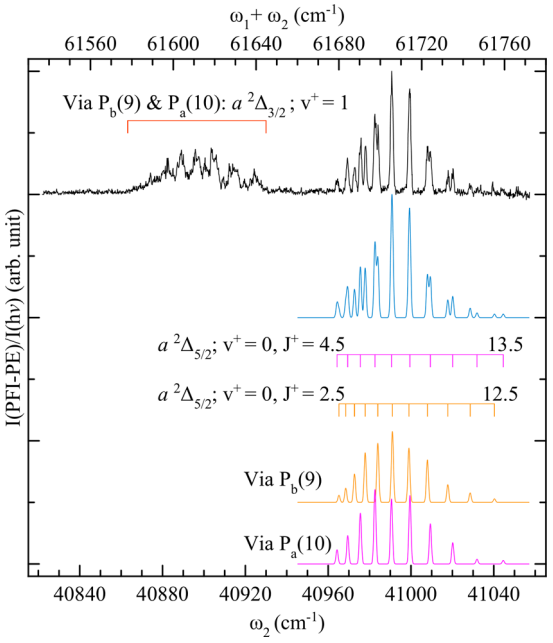

Figure 9. PFI–PE spectrum for $MoO^+(a^2\Delta_{3/2};\ v^+ = 1)$ and $MoO^+(a^2\Delta_{5/2};\ v^+ = 0)$ obtained by fixing vis ω_1 at 20 714.82 cm^{-1} and scanning UV ω_2 in the range of 40 822–41 057 cm^{-1}. The vis ω_1 excited MoO to the intermediate state $MoO^*(B^5\Pi_{-1};\ v' = 0,\ J_a' = 9$ and $J_b' = 8)$ via $P_a(10)$ and Pb(9) transitions. The blue curve is the sum of the best simulations of the $J_a' = 9 \rightarrow J^+$ and $J_b' = 8 \rightarrow J^+$ transitions, which are shown as the pink and orange curves, respectively. The simulations assume a Gaussian instrument profile of fwhm = 1.2 cm^{-1} for PFI–PE detection.

DOI: 10.1021/acs.jpca.5b07939
J. Phys. Chem. A XXXX, XXX, XXX–XXX

lowest J^+-transition peaks were not observed in the PFI−PE spectra; thus, the projection of total angular momentum J^+ on the internuclear axis Ω^+ cannot be determined unambiguously from the PFI−PE spectra. Because the $a^2\Delta_{3/2,5/2}$ states are expected to arise from the electronic configuration $\cdots(11\sigma)^2(5\pi)^4(2\delta)^1(12\sigma)^2$ (see discussion in section 3.6 below) and the 2δ orbitals are less than half-filled, we have tentatively assigned the $a^2\Delta_{3/2}$ state to lie lower than the $a^2\Delta_{5/2}$ state according to Hund's rule. The spin−orbit constant for $MoO^+(^2\Delta_{3/2})$ and $MoO^+(^2\Delta_{5/2})$ states is calculated to be 581 cm^{-1} at the CCSD(T)/aug-cc-pVTZ-DK level; but the calculation cannot determine the energy order of the $a^2\Delta_{3/2,5/2}$ fine structure states. Nevertheless, the excellent agreement observed between the latter prediction and experimental spin−orbit constant of 580.9 ± 0.8 cm^{-1} is strong support for the term symmetry assignment of $^2\Delta$ for the excited electronic state observed here.

Table 1 summarizes the energetic data and spectroscopic constants determined in the present two-color vis−UV PFI−PE measurements for the $MoO^+(X^4\Sigma^-)$ ground state and the excited low-lying $MoO^+(a^2\Delta_{3/2})$ and $MoO^+(a^2\Delta_{5/2})$ fine structure states.

Table 1. Spectroscopy Constants and Energetic Data of the MoO^+ $(X^4\Sigma^-)$ Ion Ground State and the Excited Low-Lying $a^2\Delta_{3/2,5/2}$ States

	$X^4\Sigma^-$	$a^2\Delta_{3/2}$	$a^2\Delta_{5/2}$
$v^+ = 0$			
ν_{00}^+ (cm^{-1})	60147.9 ± 0.8	60556.4 ± 0.8	61718.2 ± 0.8
IE	60095.1 ± 0.8 cm^{-1}	60556.3 ± 0.8 cm^{-1}	61718.5 ± 0.8 cm^{-1}
	7.4508 ± 0.0001 eV	7.5080 ± 0.0001 eV	7.6521 ± 0.0001 eV
B_0^+ (cm^{-1})	0.4546	0.4711	0.4695
	± 0.0006	± 0.0005	± 0.0006
λ (cm^{-1})	26.454 ± 0.017	−	−
r_0^+ (Å)	1.642 ± 0.001	1.613 ± 0.001	1.616 ± 0.001
spin−orbit constant A	−	580.9 ± 0.8 cm^{-1}	
Vibrational Constant			
$\Delta G(1/2)$ (cm^{-1})	990 ± 4	1065 ± 4	−
$\Delta G(3/2)$ (cm^{-1})	980 ± 4		−
ω_e^+ (cm^{-1})	1000 ± 9		−
$\omega_e^+x_e^+$ (cm^{-1})	5 ± 3		−
Dissociation Energy			
$D_0(Mo^+-O) - D_0(Mo-O)$ = IE(Mo) − IE(MoO)	−2890.8 ± 0.9 cm^{-1} or −0.3584 ± 0.0001 eV		

3.6. Theoretical Calculations of r_e (r_e^+) and ω_e (ω_e^+) for MoO (MoO^+). From the molecular-orbital point of view, the ground electronic state of MoO has an $^5\Pi$ symmetry, arising from the CASSCF dominant electronic configuration $0.95|(11\sigma)^2(5\pi)^4(2\delta)^2(12\sigma)^1(6\pi)^1\rangle$. The valence electrons of MoO are contributed by the $5s^14d^5$ electrons of Mo and the $2p^4$ electrons of O. Assuming that the MoO molecule lies along the z-axis, the 11σ orbital is formed by the overlap of the $Mo(4d_z^2)$ and $O(2p_z)$ orbitals. The two degenerate π bonding orbitals, $5\pi_x$ and $5\pi_y$, are formed by the overlaps of $Mo(4d_{xz})$ with $O(2p_x)$ and $Mo(4d_{yz})$ with $O(2p_y)$, respectively. The singly occupied 2δ orbitals consist of the $Mo(4d_{x^2-y^2})$ and $Mo(4d_{xy})$ orbitals, while the 12σ orbital is contributed by the Mo(5s) orbital. The 6π orbital is the antibonding $5\pi_x$ and $5\pi_y$ orbitals. On the basis of the Mulliken atomic distribution, the $MoO(X^5\Pi)$ has a triple bond, consisting of two π $(5\pi^4)$ and one σ $(11\sigma^2)$ bonds. The first ionization of $MoO(X^5\Pi)$ involves the ejection of an electron from the antibonding 6π orbital, resulting in the $MoO^+(X^4\Sigma^-)$ ground state; its CASSCF electronic configuration is $0.93|(11\sigma)^2(5\pi)^4(2\delta)^2(12\sigma)^1\rangle$.

The predicted equilibrium bond lengths r_e (r_e^+) and harmonic vibrational frequencies ω_e (ω_e^+) of $MoO(X^5\Pi)$ $[MoO^+(X^4\Sigma^-)]$ calculated at the coupled cluster, multireference configuration interaction, and B3LYP levels are summarized in Table 2. The r_e values calculated at the CCSD(T)/aug-cc-pVXZ(-PP) levels are in the range from 1.709 to 1.713 Å and are slightly shortened by ∼0.08 Å when the core−valence correlation effect is included. Similar bond lengths and vibrational frequency are also found in the CCSDT/aug-cc-pVTZ(-PP) and CCSDT/aug-cc-pVTZ-DK levels. This suggests that both the pseudopotential and all-electron basis sets (aug-cc-pVTZ-PP and aug-cc-pVTZ-DK) perform equally well. The r_e values at the CCSDT (1.713 Å), CCSDTQ (1.713 Å), and MRCI+Q (1.706 Å) levels are consistent with each other. The ω_e values calculated at the CCSD(T), CCSDT, CCSDTQ, and MRCI+Q levels are found to range from 903 to 935 cm^{-1}. No experimental values for r_e and ω_e for $MoO(X^5\Pi)$ have been reported previously.

The r_e^+, ranging from 1.634 to 1.650 Å calculated at the CCSD(T) level, comes fairly close to the experimental value of 1.642 ± 0.001 Å. The CCSDT, CCSDTQ, and MRCI+Q values (r_e^+ = 1.650, 1.651, and 1.643 Å, respectively) also correspond to the experimental value well. In the adiabatic ionization process of $MoO(X^5\Pi)$, the electron is ejected from the 6π antibonding orbital. Thus, the $MoO^+(X^4\Sigma^-)$ cation is expected to have a stronger and shorter bond along with a higher vibrational frequency. At the CCSD(T) and CCSDT level, the ω_e^+ values range from 990 to 1022 cm^{-1}; the predictions deviate from the experimental value of 1000 ± 9 cm^{-1} by ∼10−22 cm^{-1}. The ω_e^+ value of 974 cm^{-1} obtained at the CCSDTQ level is 26 cm^{-1} lower than the experimental value. Overall, the MRCI+Q r_e^+ value of 1.643 Å and ω_e^+ value of 997 cm^{-1} give the best agreement with the experimental PFI−PE values.

3.7. Theoretical Values for IE(MoO), D_0(Mo−O), $D_0(Mo^+-O)$, $\Delta H°_{ft}$(MoO), and $\Delta H°_{ft}(MoO^+)$. It is of great interest to examine the performance of single-reference coupled cluster theory in energetic predictions for the MoO/MoO^+ system, which possesses closely spaced low-lying excited multiplicity states. The individual energy corrections ($\Delta E_{extrapolated\ CBS}$, ΔE_{CV}, ΔE_{ZPVE}, ΔE_{SO}, and ΔE_{HOC}) for the IE(MoO), IE(Mo), D_0(Mo−O), and $D_0(Mo^+-O)$ predictions using the CCSDTQ/CBS method are listed in Table 3. The CCSDTQ/CBS prediction for IE(MoO) = 7.457 eV is found to be 6 meV larger than the measured IE(MoO) = 7.4508 ± 0.0001 eV. The most significant contribution (ΔE_{SO} = 30 meV) to IE(MoO) is the spin−orbit coupling correction. The CCSDTQ/CBS procedure also gives an excellent prediction to the IE(Mo) value of 7.086 eV, which differs from the experimental value[43] of 7.09243 ± 0.00004 eV by ∼6 meV.

On the basis of the CCSDTQ/CBS values of IE(MoO) = 7.457 and IE(Mo) = 7.086 eV, we obtain a theoretical $D_0(Mo^+-O) - D_0$(Mo−O) value of −0.371 eV. This predicted value for $D_0(Mo^+-O) - D_0$(Mo−O) is in excellent agreement with the present PFI−PE experimental value of −0.3584 ± 0.0001 eV. The experimental values D_0(Mo−O) = 5.76 ± 0.22

DOI: 10.1021/acs.jpca.5b07939
J. Phys. Chem. A XXXX, XXX, XXX−XXX

Table 2. Bond Length, r_e (r_e^+), and Harmonic Vibrational Frequency, ω_e (ω_e^+), for MoO($X^5\Pi$)/MoO^+($X^4\Sigma^-$) Predicted at the CCSD(T), CCSDT, CCSDTQ, MRCI+Q, and B3LYP Using aug-cc-p(wC)VXZ(-PP) Levels, Where X = T, Q, and 5

	MoO($^5\Pi$)		MoO^+($^4\Sigma^-$)	
	r_e (Å)	ω_e (cm^{-1})	r_e^+ (Å)	ω_e^+ (cm^{-1})
CCSD(T)/aug-cc-pVTZ-DK	1.711	919	1.648	994
CCSD(T)/aug-cc-pVTZ(-PP)	1.713	915	1.650	990
CCSD(T)/aug-cc-pVQZ(-PP)	1.709	921	1.646	995
CCSD(T)/aug-cc-pV5Z(-PP)	1.707	924	1.644	997
CCSD(T)/aug-cc-pwCVTZ(-PP)[a]	1.704	925	1.639	1016
CCSD(T)/aug-cc-pwCVQZ(-PP)[a]	1.701	931	1.635	1019
CCSD(T)/aug-cc-pwCV5Z(-PP)[a]	1.699	935	1.634	1022
CCSDT/aug-cc-pVTZ(-PP)	1.713	917	1.650	990
CCSDTQ/cc-pVTZ(-PP)	1.713	903	1.651	974
MRCI+Q/aug-cc-pwCVTZ(-PP)[a]	1.706	921	1.643	997
B3LYP/aug-cc-pVTZ(-PP)	1.700	954	1.629	1059
exptl			1.642 ± 0.001	1000 ± 9

[a]Correlated with the 4s4p4d5s (Mo) and 1s2s2p (O) electrons.

Table 3. Individual Energy Contributions to the CCSDTQ/CBS Predictions for the IE(MoO), IE(Mo), D_0(Mo−O), and $D_0(Mo^+-O)$ Values[a]

		IE(MoO)	IE(Mo)	D_0(Mo−O)	$D_0(Mo^+-O)$	$D_0(Mo^+-O) - D_0$(Mo−O)
$\Delta E_{extrapolatedCBS}$[b]	eq 1	7.424	7.088	5.377	5.041	−0.336
	eq 2	7.428	7.086	5.395	5.053	−0.342
	average	7.426	7.087	5.386	5.047	−0.339
ΔE_{CV}[c]	(T) → T	−0.010	−0.006	0.012	0.016	0.004
ΔE_{ZPVE}[d]		0.004	/	−0.056	−0.060	−0.004
ΔE_{SO}[e]		0.030	0.000	0.034	0.004	−0.030
ΔE_{HOC}[f]	(T) → T	0.014	0.004	−0.026	−0.036	−0.010
	T → Q	−0.007	0.001	0.036	0.044	0.008
	subtotal	0.007	0.005	0.010	0.008	−0.002
CCSDTQ/CBS[g]		7.457	7.086	5.386	5.015	−0.371
exptl		7.4508 ± 0.0001[h]	7.09243 ± 0.00004[i]	5.76 ± 0.22[j]	5.40 ± 0.22[j]	−0.3584 ± 0.0001[h]
				5.42 ± 0.02[k]	5.06 ± 0.02[k]	

[a]All quantities and energy differences are in electronvolts. [b]Extrapolated from the CCSD(T) energies using eqs 1 and 2. [c]Core−valence electronic correlation obtained as the energy difference between CCSD(T) and CCSDT levels using the cc-pwCVTZ(-PP) basis set. [d]Based on the harmonic vibrational frequencies at the CCSDTQ/cc-pVTZ(-PP) level. [e]Spin−orbit coupling obtained at the MRCI level with the aug-cc-pVTZ-DK basis set. [f]Higher-order effect calculated at the CCSDT/aug-cc-pVQZ(-PP) and CCSDTQ/cc-pVTZ(-PP) levels. [g]IE or D_0 = $\Delta E_{extrapolated\ CBS}$ + ΔE_{CV} + ΔE_{ZPVE} + ΔE_{SO} + ΔE_{HOC}. [h]This work. [i]From ref 43. [j]D_0(Mo−O) = 5.76 ± 0.22 eV is taken from ref 49; the $D_0(Mo^+-O)$ value is derived using the IE(MoO) = 7.4508 ± 0.0001 and IE(Mo) = 7.09243 ± 0.00004 eV. [k]$D_0(Mo^+-O)$ = 5.06 ± 0.02 eV is taken from ref 50; the D_0(Mo−O) value is derived using the IE(MoO) and IE(Mo).

eV and $D_0(Mo^+-O)$ = 5.06 ± 0.02 eV have been reported previously by Pedley and Marshall[49] and Armentrout and co-workers,[50] respectively. By combining the experimental $D_0(Mo^+-O) - D_0$(Mo−O) = −0.3584 ± 0.0001 eV and D_0(Mo−O) = 5.76 ± 0.22 eV, we deduced an experimental value of 5.40 ± 0.22 for $D_0(Mo^+-O)$. Similarly, an experimental value of D_0(Mo−O) = 5.42 ± 0.02 eV can be obtained by using $D_0(Mo^+-O)$ = 5.06 ± 0.02 eV. These experimental D_0 values deduced here are also included in Table 3. The CCSDTQ/CBS predictions of D_0(Mo−O) = 5.386 and $D_0(Mo^+-O)$ = 5.015 eV are more consistent with the experimental values D_0(Mo−O) = 5.42 ± 0.02 eV and $D_0(Mo^+-O)$ = 5.06 ± 0.02 eV. The above comparison indicates that the D_0(Mo−O) value reported by Pedley and Marshall[49] is likely too high.

There are several experimental ΔH°_{fT} values for MoO and MoO^+ available in the literature: (i) ΔH°_{f0}(MoO) = 310.3 ± 33.5 and ΔH°_{f298}(MoO) = 311.0 ± 33.5 kJ mol^{-1} from JANAF thermochemical data[42] and (ii) ΔH°_{f298}(MoO) = 347 ± 21 kJ mol^{-1} reported by Pedley and Marshall.[49] On the basis of the present IE(MoO) = 7.4508 ± 0.0001 eV, the known values for ΔH°_{f0}(Mo) = 656.6, ΔH°_{f298}(Mo) = 658.1, ΔH°_{f0}(O) = 246.8, and ΔH°_{f298}(O) = 249.2 kJ mol^{-1}, along with the 298 K thermal corrections from the CCSDTQ vibrational frequencies of MoO/MoO^+, we derived two sets of experimental ΔH°_{f0} and ΔH°_{f298} values (Table 4): (i) ΔH°_{f0}(MoO) = 310.3 ± 33.5, ΔH°_{f298}(MoO) = 311.0 ± 33.5, $\Delta H^\circ_{f0}(MoO^+)$ = 1029.2 ± 33.5, and $\Delta H^\circ_{f298}(MoO^+)$ = 1029.5 ± 33.5 kJ mol^{-1}; (ii) ΔH°_{f0}(MoO) = 347 ± 21, ΔH°_{f298}(MoO) = 347 ± 21, $\Delta H^\circ_{f0}(MoO^+)$ = 1066 ± 21, and $\Delta H^\circ_{f298}(MoO^+)$ = 1066 ± 21 kJ mol^{-1}. Compared with the CCSDTQ/CBS predictions of ΔH°_{f0}(MoO) = 383.7, ΔH°_{f298}(MoO) = 384.0, $\Delta H^\circ_{f0}(MoO^+)$ = 1103.2, and $\Delta H^\circ_{f298}(MoO^+)$ = 1103.5 kJ mol^{-1}, these two sets of experimental ΔH°_{fT} values are consistently smaller than CCSDTQ/CBS values by ∼70 and ∼40 kJ mol^{-1}, respectively. This suggests that the previous reported experimental ΔH°_{fT} values have fairly large uncertainties. However, if the experimental $D_0(Mo^+-O)$ = 5.06 ± 0.02 eV[50] is used, the set of experimental values (Table 4) for ΔH°_{f0}(MoO) = 380.5 ± 1.9, ΔH°_{f298}(MoO) = 380.8 ± 1.9, $\Delta H^\circ_{f0}(MoO^+)$ = 1099.4 ±

DOI: 10.1021/acs.jpca.5b07939
J. Phys. Chem. A XXXX, XXX, XXX−XXX

Table 4. Individual Energy Contributions to the CCSDTQ/CBS Atomization Energies, ΔH°_{f0} and ΔH°_{f298} Values for MoO/MoO$^+$[a]

		MoO	MoO$^+$
$\Delta E_{\text{extrapolatedCBS}}$[b]	eq 1	518.8	−197.5
	eq 2	520.6	−196.1
	average	519.7	−196.8
ΔE_{CV}[c]	(T) → T	1.1	2.1
ΔE_{ZPVE}		−5.4	−5.8
ΔE_{SO}[d]		3.3	0.4
ΔE_{HOC}[e]	(T) → T	−2.5	−3.9
	T → Q	3.5	4.2
	subtotal	1.0	0.3
CCSDTQ/CBS $\sum D_0$[f]		519.7	−199.8
CCSDTQ/CBS ΔH°_{f0}[g]		383.7	1103.2
CCSDTQ/CBS ΔH°_{f298}[h]		384.0	1103.5
exptl ΔH°_{f0}		310.3 ± 33.5[i] ≈347 ± 21[j] 380.5 ± 1.9[k]	1029.2 ± 33.5[i] ≈1066 ± 21[j] 1099.4 ± 1.9[k]
exptl ΔH°_{f298}		311.0 ± 33.5[i] 347 ± 21[j] 380.8 ± 1.9[k]	1029.5 ± 33.5[i] ≈1066 ± 21[j] 1099.7 ± 1.9[k]

[a]All quantities and energy differences are in kilojoules per mole. [b]Extrapolated from the CCSD(T) energies using eqs 1 and 2. [c]Core−valence electronic correlation obtained as the energy difference between CCSD(T) and CCSDT levels using the cc-pwCVTZ(-PP) basis set. [d]Spin−orbit coupling obtained at the MRCI level with the aug-cc-pVTZ-DK level. [e]Higher-order effect calculated at the CCSDT/aug-cc-pVQZ(-PP) and CCSDTQ/cc-pVTZ(-PP) levels. [f]$\sum D_0 = \Delta E_{\text{extrapolated CBS}} + \Delta E_{CV} + \Delta E_{ZPVE} + \Delta E_{SO} + \Delta E_{HOC}$. [g]$\Delta H^\circ_{f0} = \Delta H^\circ_{f0}(\text{Mo}) + \Delta H^\circ_{f0}(\text{O}) - \sum D_0$. [h]$\Delta H^\circ_{f298} = \Delta H^\circ_{f298}(\text{Mo}) + \Delta H^\circ_{f298}(\text{O}) - \sum D_0$ − thermal and enthalpy corrections. [i]Experimental $\Delta H^\circ_{f0}(\text{MoO}) = 310.3 \pm 33.5$ and $\Delta H^\circ_{f298}(\text{MoO}) = 311.0 \pm 33.5$ kJ mol^{-1} are taken from ref 42. The $\Delta H^\circ_{f0}(\text{MoO}^+)$ and $\Delta H^\circ_{f298}(\text{MoO}^+)$ are deduced from IE(MoO) = 7.4508 ± 0.0001 eV, $\Delta H^\circ_{f0}(\text{Mo}) = 656.6$, $\Delta H^\circ_{f298}(\text{Mo}) = 658.1$, $\Delta H^\circ_{f0}(\text{O}) = 246.8$, and $\Delta H^\circ_{f298}(\text{O}) = 249.2$ kJ mol^{-1} (ref 42). [j]Experimental $\Delta H^\circ_{f298}(\text{MoO}) = 347 \pm 21$ kJ mol^{-1} are taken from ref 49. The $\Delta H^\circ_{f0}(\text{MoO})$, $\Delta H^\circ_{f0}(\text{MoO}^+)$, and $\Delta H^\circ_{f298}(\text{MoO}^+)$ are deduced from IE(MoO) and ΔH°_f values of Mo and O; all values are rounded up to no decimal place. [k]Deduced from $D_0(\text{Mo}^+-\text{O}) = 5.06 \pm 0.02$ eV (ref 50) and IE(MoO) and ΔH°_f values of Mo and O.

1.9, and $\Delta H^\circ_{f298}(\text{MoO}^+) = 1099.7 \pm 1.9$ kJ mol^{-1} is obtained. This set of experimental ΔH°_{fT} values is consistent with the CCSDTQ/CBS predictions with deviations less than 4 kJ mol^{-1}.

4. CONCLUSION

By performing two-color vis−UV PFI−PE measurements, we have obtained rotationally resolved state-to-state photoelectron spectra for MoO$^+$($X^4\Sigma^-$; $v^+ = 0$, 1, and 2) and Mo($a^2\Delta_{3/2,5/2}$; $v^+ = 0$ and 1). The unambiguous rotational assignments have allowed the determination of the band origin $\nu^+_{00} = 60\,147.9 \pm 0.8$ cm^{-1}, rotation constant $B_0^+ = 0.4546 \pm 0.0006$ cm^{-1}, spin−spin coupling constant $\lambda = 26.454 \pm 0.017$ cm^{-1}, and the bond length $r_0^+ = 1.642 \pm 0.001$ Å for MoO$^+$ ($X^4\Sigma^-$); $\nu^+_{00} = 60\,556.4 \pm 0.8$ cm^{-1}, $B_0^+ = 0.4711 \pm 0.0005$ cm^{-1}, and $r_0^+ = 1.613 \pm 0.001$ Å for MoO$^+$($a^2\Delta_{3/2}$); and $\nu^+_{00} = 61\,715.2 \pm 0.8$ cm^{-1}, $B_0^+ = 0.4695 \pm 0.0006$ cm^{-1}, and $r_0^+ = 1.616 \pm 0.001$ Å for MoO$^+$($a^2\Delta_{5/2}$). From the present PFI−PE measurement of MoO$^+$($X^4\Sigma^-$; $v^+ = 0$−2), the IE(MoO) is determined to be 60 095.1 ± 0.8 cm^{-1} or 7.4508 ± 0.0001 eV. Furthermore, the harmonic vibrational frequency and anharmonicity constant are determined to be $\omega_e^+ = 1000 \pm 9$ cm^{-1} and $\omega_e^+ x_e^+ = 5 \pm 3$ cm^{-1}, respectively, for MoO$^+$($X^4\Sigma^-$). The vibration spacing $\Delta G(1/2)$ for MoO$^+$($a^2\Delta_{3/2}$) is determined to be 1065 ± 4 cm^{-1}. From a thermochemical cycle, together with the known IE(Mo) and the IE(MoO) determined in this study, the difference of 0 K bond dissociation energy for MoO$^+$ and that for MoO is determined as $D_0(\text{Mo}^+-\text{O}) - D_0(\text{Mo}-\text{O}) = \text{IE(Mo)} - \text{IE(MoO)} = -2890.8 \pm 0.9$ cm^{-1} or −0.3584 ± 0.0001 eV. The IE value, 0 K bond dissociation energy difference, together with the spectroscopy constants and bond length determined here have been used to benchmark predictions obtained based on the CCSDTQ/CBS procedure. The CCSDTQ/CBS prediction of IE(MoO) = 7.457 eV is in excellent agreement with the value determined by the PFI−PE measurement. The CCSDTQ values for $r_e^+ = 1.651$ Å and $\omega_e^+ = 974$ cm^{-1} are also in good accord with the experimental $r_e^+ = 1.642 \pm 0.001$ Å and $\omega_e^+ = 1000 \pm 9$ cm^{-1}. The current available experimental ΔH°_{f0} and ΔH°_{f298} values[42,49] for MoO and MoO$^+$ are found to deviate from the CCSDTQ/CBS values by 40−70 kJ mol^{-1}, suggesting that the experimental ΔH°_{f0} and ΔH°_{f298} values are likely to have large uncertainties. The excellent agreement observed between the CCSDTQ/CBS predictions and current experimental energetic measurements, including IE(MoO) and $D_0(\text{Mo}^+-\text{O}) - D_0(\text{Mo}-\text{O})$ values, suggests that the CCSDTQ/CBS predictions of $D_0(\text{Mo}-\text{O}) = 5.386$ eV, $D_0(\text{Mo}^+-\text{O}) = 5.015$ eV, $\Delta H^\circ_{f0}(\text{MoO}) = 383.7$ kJ/mol, $\Delta H^\circ_{f298}(\text{MoO}) = 384.0$ kJ/mol, $\Delta H^\circ_{f0}(\text{MoO}^+) = 1103.2$ kJ/mol, and $\Delta H^\circ_{f298}(\text{MoO}^+) = 1103.5$ kJ/mol are equally reliable.

AUTHOR INFORMATION

Corresponding Authors

*E-mail: kaichung@cityu.edu.hk. Tel:+(852)-3442-6849.

*E-mail: cyng@chem.ucdavis.edu. Tel: +1(530)-754-9645.

Notes

The authors declare no competing financial interest.

ACKNOWLEDGMENTS

This material is based upon work supported by the National Science Foundation under CHE-0910488 and CHE-1462172.

REFERENCES

(1) Chang, Y. C.; Lam, C. S.; Reed, B.; Lau, K. C.; Liou, H.; Ng, C. Rovibronically Selected and Resolved Two-Color Laser Photoionization and Photoelectron Study of the Iron Carbide Cation. *J. Phys. Chem. A* **2009**, *113*, 4242−4248.

(2) Chang, Y. C.; Shi, X.; Lau, K. C.; Yin, Q. Z.; Liou, H.; Ng, C. Rovibronically Selected and Resolved Two-Color Laser Photoionization and Photoelectron Study of Nickel Carbide Cation. *J. Chem. Phys.* **2010**, *133*, 054310.

(3) Huang, H.; Chang, Y. C.; Luo, Z.; Shi, X.; Lam, C.-S.; Lau, K.-C.; Ng, C. Rovibronically Selected and Resolved Two-Color Laser Photoionization and Photoelectron Study of Cobalt Carbide Cation. *J. Chem. Phys.* **2013**, *138*, 094301.

(4) Luo, Z.; Huang, H.; Chang, Y.-C.; Zhang, Z.; Yin, Q.-Z.; Ng, C. Y. Rotationally Resolved State-to-State Photoionization and Photoelectron Study of Titanium Carbide and Its Cation (TiC/TiC$^+$). *J. Chem. Phys.* **2014**, *141*, 144307.

(5) Huang, H.; Luo, Z.; Chang, Y. C.; Lau, K.-C.; Ng, C. Rovibronically Selected and Resolved Two-Color Laser Photoionization and Photoelectron Study of Titanium Monoxide Cation. *J. Chem. Phys.* **2013**, *138*, 174309.

DOI: 10.1021/acs.jpca.5b07939
J. Phys. Chem. A XXXX, XXX, XXX−XXX

(6) Chang, Y. C.; Luo, Z.; Pan, Y.; Zhang, Z.; Song, Y.-N.; Kuang, S. Y.; Yin, Q. Z.; Lau, K.-C.; Ng, C. Y. Rotationally Resolved State-to-State Photoionization and the Photoelectron Study of Vanadium Monocarbide and Its Cations (VC/VC$^+$). *Phys. Chem. Chem. Phys.* **2015**, *17*, 9780−9793.
(7) Huang, H.; Luo, Z. h.; Chang, Y. C.; Lau, K. C.; Ng, C. Y. State-to-State Photoionization Dynamics of Vanadium Nitride by Two-Color Laser Photoionization and Photoelectron Methods. *Chin. J. Chem. Phys.* **2013**, *26*, 669−678.
(8) Lau, K. C.; Chang, Y. C.; Lam, C. S.; Ng, C. High-Level Ab Initio Predictions for the Ionization Energy, Bond Dissociation Energies, and Heats of Formations of Iron Carbide (FeC) and Its Cation (FeC$^+$). *J. Phys. Chem. A* **2009**, *113*, 14321−14328.
(9) Lau, K.-C.; Chang, Y. C.; Shi, X.; Ng, C. Y. High-Level Ab Initio Predictions for the Ionization Energy, Bond Dissociation Energies, and Heats of Formation of Nickel Carbide (NiC) and Its Cation (NiC$^+$). *J. Chem. Phys.* **2010**, *133*, 114304.
(10) Lau, K.-C.; Pan, Y.; Lam, C.-S.; Huang, H.; Chang, Y.-C.; Luo, Z.; Shi, X.; Ng, C. Y. High-Level Ab Initio Predictions for the Ionization Energy, Bond Dissociation Energies, and Heats of Formation of Cobalt Carbide (CoC) and Its Cation (CoC$^+$). *J. Chem. Phys.* **2013**, *138*, 094302.
(11) Luo, Z.; Huang, H.; Zhang, Z.; Chang, Y. C.; Ng, C. Y. Rotationally Resolved State-to-State Photoelectron Study of Niobium Carbide Radical. *J. Chem. Phys.* **2014**, *141*, 024304.
(12) Luo, Z.; Chang, Y.-C.; Zhang, Z.; Ng, C. Y. Rotationally Resolved State-to-State Photoelectron Study of Zirconium Monoxide Cation (ZrO$^+$). *Mol. Phys.* **2015**, *113*, 2228−2242.
(13) Hamrick, Y. M.; Taylor, S.; Morse, M. D. Optical Spectroscopy of Jet-Cooled MoO. *J. Mol. Spectrosc.* **1991**, *146*, 274−313.
(14) Kuzyakov, Y. Y.; Moskvitina, E. N.; Filippova, E. N. Intracavity Electronic Absorption Spectra of MoO and WO Molecules in the Visible Region. *Spectrosc. Lett.* **1997**, *30*, 1057−1066.
(15) Harms, J. C.; Womack, K. A.; O'Brien, L. C.; Zou, W. Analysis of a New MoO Transition in the near-Ir: A Combined Theoretical and Experimental Study. *J. Chem. Phys.* **2014**, *141*, 134310.
(16) Gunion, R. F.; Lineberger, W. C.; Morse, M. D. Ultraviolet Photoelectron Spectroscopy of Molybdenum and Molybdenum Monoxide Anions. *J. Chem. Phys.* **1996**, *104*, 1765−1773.
(17) Loock, H.-P.; Simard, B.; Wallin, S.; Linton, C. Ionization Potentials and Bond Energies of TiO, ZrO, NbO and MoO. *J. Chem. Phys.* **1998**, *109*, 8980−8992.
(18) Bauschlicher, C. W., Jr; Nelin, C. J.; Bagus, P. S. Transition Metal Oxides: CrO, MoO, NiO, PdO, AgO. *J. Chem. Phys.* **1985**, *82*, 3265−3276.
(19) Langhoff, S. R.; Bauschlicher, C. W., Jr; Pettersson, L. G. M.; Siegbahn, P. E. M. Theoretical Spectroscopic Constants for the Low-Lying States of the Oxides and Sulfides of Mo and Tc. *Chem. Phys.* **1989**, *132*, 49−57.
(20) Brocławik, E.; Salahub, D. R. On the Electronic Structure of MoO: Spin-Polarized Density Functional Calculations of Spectroscopic Properties of Low-Lying Quintet, Triplet, and Septet States. *Int. J. Quantum Chem.* **1994**, *52*, 1017−1026.
(21) Brocławik, E.; Borowski, T. Time-Dependent DFT Study on Electronic States of Vanadium and Molybdenum Oxide Molecules. *Chem. Phys. Lett.* **2001**, *339*, 433−437.
(22) Gong, Y.; Zhou, M.; Andrews, L. Spectroscopic and Theoretical Studies of Transition Metal Oxides and Dioxygen Complexes. *Chem. Rev.* **2009**, *109*, 6765−6808.
(23) Watts, J. D.; Gauss, J.; Bartlett, R. J. Coupled-Cluster Methods with Noniterative Triple Excitations for Restricted Open-Shell Hartree−Fock and Other General Single Determinant Reference Functions. Energies and Analytical Gradients. *J. Chem. Phys.* **1993**, *98*, 8718−8733.
(24) Rittby, M.; Bartlett, R. J. An Open-Shell Spin-Restricted Coupled Cluster Method: Application to Ionization Potentials in Nitrogen. *J. Phys. Chem.* **1988**, *92*, 3033−3036.
(25) Peterson, K. A.; Figgen, D.; Dolg, M.; Stoll, H. Energy-Consistent Relativistic Pseudopotentials and Correlation Consistent Basis Sets for the 4d Elements Y−Pd. *J. Chem. Phys.* **2007**, *126*, 124101.
(26) Peterson, K. A.; Dunning, T. H., Jr Accurate Correlation Consistent Basis Sets for Molecular Core−Valence Correlation Effects: The Second Row Atoms Al−Ar, and the First Row Atoms B−Ne Revisited. *J. Chem. Phys.* **2002**, *117*, 10548−10560.
(27) Peterson, K. A.; Woon, D. E.; Dunning, T. H., Jr Benchmark Calculations with Correlated Molecular Wave Functions. Iv. The Classical Barrier Height of the H+ H_2→ H_2+ H Reaction. *J. Chem. Phys.* **1994**, *100*, 7410−7415.
(28) Helgaker, T.; Klopper, W.; Koch, H.; Noga, J. Basis-Set Convergence of Correlated Calculations on Water. *J. Chem. Phys.* **1997**, *106*, 9639−9646.
(29) Halkier, A.; Helgaker, T.; Jørgensen, P.; Klopper, W.; Koch, H.; Olsen, J.; Wilson, A. K. Basis-Set Convergence in Correlated Calculations on Ne, N_2, and H_2O. *Chem. Phys. Lett.* **1998**, *286*, 243−252.
(30) Lau, K. C.; Ng, C. Y. Accurate Ab Initio Predictions of Ionization Energies of Hydrocarbon Radicals: CH_2, CH_3, C_2H, C_2H_3, C_2H_5, C_3H_3, and C_3H_5. *J. Chem. Phys.* **2005**, *122*, 224310.
(31) Lau, K.-C.; Ng, C.-Y. Benchmarking State-of-the-Art Ab Initio Thermochemical Predictions with Accurate Pulsed-Field Ionization Photoion-Photoelectron Measurements. *Acc. Chem. Res.* **2006**, *39*, 823−829.
(32) Lau, K. C.; Ng, C.-Y. Accurate Ab Initio Predictions of Ionization Energies and Heats of Formation for Cyclopropenylidene, Propargylene and Propadienylidene. *Huaxue Wuli Xuebao* **2006**, *19*, 29−38.
(33) Lau, K. C.; Ng, C. Y. Accurate Ab Initio Predictions of Ionization Energies and Heats of Formation for the 2-Propyl, Phenyl, and Benzyl Radicals. *J. Chem. Phys.* **2006**, *124*, 044323.
(34) Lau, K.-C.; Ng, C. Y. Note: Accurate Ab Initio Predictions of Ionization Energies of Propargyl and Allyl Radicals: Revisited. *J. Chem. Phys.* **2011**, *135*, 246101.
(35) Berning, A.; Schweizer, M.; Werner, H.-J.; Knowles, P. J.; Palmieri, P. Spin-Orbit Matrix Elements for Internally Contracted Multireference Configuration Interaction Wavefunctions. *Mol. Phys.* **2000**, *98*, 1823−1833.
(36) Whaling, W.; Brault, J. W. Comprehensive Transition Probabilities in Mo I. *Phys. Scr.* **1988**, *38*, 707.
(37) Kiess, C. C. *J. Res. Natl. Bur. Stand.(U.S.)* **1958**, *60*, 375.
(38) Moore, C. E. *Atomic Energy Levels*; Natl. Bur. Stand. (U.S.) Circular No. 467; U.S. Government Printing Office: Washington, DC, 1949.
(39) Werner, H.-J.; et al. *MOLPRO*, version 2010.1, a package of ab initio programs, 2010. See http://www.molpro.net.
(40) Kállay, M. A String-Based Quantum Chemical Program Suite, 2001. See also Surján, P. R. Higher Excitations in Coupled-Cluster Theory. *J. Chem. Phys.*, **2001**, *115*, 2945 10.1063/1.1383290 as well as http://www.mrcc.hu.
(41) Curtiss, L. A.; Raghavachari, K.; Redfern, P. C.; Pople, J. A. Assessment of Gaussian-2 and Density Functional Theories for the Computation of Enthalpies of Formation. *J. Chem. Phys.* **1997**, *106*, 1063−1079.
(42) *NIST-JANAF Thermochemical Tables*; Chase, M. W., Ed.; J. Phys. Chem. Ref. Data. Monograph; American Chemical Society: Washington, DC, 1998
(43) Rayner, D. M.; Mitchell, S. A.; Bourne, O. L.; Hackett, P. A. First-Ionization Potential of Niobium and Molybdenum by Double-Resonance, Field-Ionization Spectroscopy. *J. Opt. Soc. Am. B* **1987**, *4*, 900−905.
(44) Western, C. M.PGOPHER, a Program for Simulating Rotational Structure; University of Bristol; http://pgopher.chm.bris.ac.uk.
(45) Schlag, E. W. *ZEKE Spectroscopy*; Cambridge University Press: Cambridge, 1996.
(46) Luo, Z.; Zhang, Z.; Huang, H.; Chang, Y. C.; Ng, C. Y. State-to-State Photoionization and Photoelectron Study of Vanadium Methylidyne Radical (VCH). *J. Chem. Phys.* **2014**, *140*, 181101.

DOI: 10.1021/acs.jpca.5b07939
J. Phys. Chem. A XXXX, XXX, XXX−XXX

(47) Merkt, F.; Softley, T. P. Rotational Line Intensities in Zero Kinetic Energy Photoelectron Spectroscopy (Zeke-Pes). *Int. Rev. Phys. Chem.* **1993**, *12*, 205−239.
(48) Linton, C.; Simard, B.; Loock, H. P.; Wallin, S.; Rothschopf, G. K.; Gunion, R. F.; Morse, M. D.; Armentrout, P. B. Rydberg and Pulsed Field Ionization-Zero Electron Kinetic Energy Spectra of YO. *J. Chem. Phys.* **1999**, *111*, 5017.
(49) Pedley, J. B.; Marshall, E. M. Thermochemical Data for Gaseous Monoxides. *J. Phys. Chem. Ref. Data* **1983**, *12*, 967.
(50) Sievers, M. R.; Chen, Y. M.; Armentrout, P. B. Metal Oxide and Carbide Thermochemistry of Y^+, Zr^+, Nb^+, and Mo^+. *J. Chem. Phys.* **1996**, *105*, 6322−6333.

DOI: 10.1021/acs.jpca.5b07939
J. Phys. Chem. A XXXX, XXX, XXX−XXX